Regulation of blood cell transdifferentiation by oxygen sensing neurons in *Drosophila*

Sean Corcoran[2], Anjeli Mase[2], Yousuf Hashmi[2], Debra Ouyang[2], Jordan Augsburger[2], Thea Jacobs[2], Katelyn Kukar[2], Katja Brückner[1, 2, 3, 4]

[1]Eli and Edythe Broad Center of Regeneration Medicine and Stem Cell Research

[2]Department of Cell and Tissue Biology

[3]Cardiovascular Research Institute, University of California San Francisco, San Francisco, CA

[4] Corresponding Author:

35 Medical Center Way

San Francisco, CA 94143-066

e-mail: katja.brueckner@ucsf.edu

Highlights

- Functional lineage tracing reveals in vivo transdifferentiation in a *Drosophila* model of hematopoiesis
- Active sensory neurons of the caudal sensory cones promote blood cell transdifferentiation in the *Drosophila* larva
- Environmental oxygen sensing through atypical guanylyl cyclases in sensory cone neurons drives blood cell transdifferentiation

Keywords

Drosophila melanogaster, transdifferentiation, hematopoiesis, microenvironment, hemocyte, macrophage, plasmatocyte, crystal cell, sensory neurons, sensory cones, atypical guanylyl cyclase, oxygen sensing, hypoxia

Summary

Transdifferentiation generates functionally specialized cell types independent of stem or progenitor cells. Despite the unique nature of the process, it remains poorly understood how transdifferentiation is regulated in vivo. Here we reveal a mechanism of environmental control of blood cell transdifferentiation in a *Drosophila melanogaster* model of hematopoiesis. Using functional lineage tracing, we find in vivo evidence for transdifferentiation from macrophage-like plasmatocytes to crystal cells that execute melanization. Interestingly, this transdifferentiation is promoted by neuronal activity of a specific subset of sensory neurons, in the sensory cones at the caudal end of the larva, as is evidenced through genetic ablation, and manipulation of neuronal activity by *Kir2.1* and *TrpA1*. Crystal cells develop from plasmatocyte clusters surrounding the sensory cones. Strikingly, environmental conditions trigger this process: oxygen sensing, through atypical guanylyl cyclases (Gyc88E, Gyc89Da, Gyc89Db) that are specifically expressed in sensory cone neurons, drives plasmatocyte-to-crystal cell transdifferentiation, as hypoxia or *Gyc* silencing cause crystal cell reduction and loss of transdifferentiation. Our findings reveal an unexpected functional and molecular link of environment-monitoring sensory neurons that govern blood cell transdifferentiation in vivo, suggesting similar principles in vertebrate systems where environmental sensors and blood cell populations coincide.

Introduction

A Drosophila model of blood cell transdifferentiation

The phenomenon of transdifferentiation has been noted in a variety of species (Cieslar-Pobuda et al., 2017; Graf, 2011; Reid and Tursun, 2018), yet its in vivo regulation remains poorly understood. In the vertebrate blood cell system, reports of transdifferentiation have for the most part been limited to cell culture systems and experimental manipulations. For example, C/EBP (CCAAT/enhancer-binding protein) transcription factors drive transdifferentiation of vertebrate B cells to macrophages (Xie et al., 2004) (Di Tullio et al., 2011), B lymphoma and leukemia cell lines to macrophages (Rapino et al., 2013), and B cells to Granulocyte-Macrophage Precursors (Cirovic et al., 2017). Similarly, manipulation of key transcription factors such as FLI1 and ERG results in transdifferentiation of erythroblasts to megakaryocytes (Siripin et al., 2015), and deletion of the BAF Chromatin Remodeling Complex Subunit Bcl11b triggers T cell transition to NK cells (Li et al., 2010). Transdifferentiation of lymphoid and myeloid cells has been modeled mathematically (Collombet et al., 2017). However, in vivo, the underlying cellular and molecular mechanisms of blood cell transdifferentiation during development and homeostasis and the role of the environment remain elusive.

To investigate principles of in vivo transdifferentiation in the hematopoietic system, we turned to a model in *Drosophila melanogaster*. *Drosophila* offers proven parallels to the two major lineages that produce myeloid blood cells in vertebrates (Davies et al., 2013; Perdiguero and Geissmann, 2016; Sieweke and Allen, 2013), with its two myeloid lineages of blood cells, or hemocytes (Gold and Brückner, 2014, 2015; Holz et al., 2003), (1) the embryonic lineage of hemocytes that proliferate as differentiated cells in hematopoietic pockets of the larval body wall, and resemble vertebrate tissue macrophages, and (2) the progenitor-based lymph gland lineage (Banerjee et al., 2019). Both *Drosophila* blood cell lineages produce at least three differentiated blood cell types: macrophage-like plasmatocytes, crystal cells that mediate melanization, and lamellocytes, large immune cells specialized for encapsulation (Banerjee et al., 2019; Gold and Brückner, 2014, 2015). During larval stages, embryonic-lineage plasmatocytes show signs of fate changes to other blood cell types: Transdifferentiation to lamellocytes occurs in response to immune challenges (Markus et al., 2009), and transdifferentiation to crystal cells was suggested even under steady state conditions (Leitao and Sucena, 2015). However, it remains unclear what are the anatomical requirements and environmental inputs that regulate plasmatocyte-to-crystal cell transdifferentiation in vivo. Hematopoietic sites of

52 the *Drosophila* larva contain sensory neuron clusters of the peripheral nervous system (PNS) that
53 serve as microenvironments for plasmatocyte survival, proliferation and localization (Gold and
54 Brückner, 2014, 2015; Makhijani et al., 2017; Makhijani et al., 2011; Makhijani and Brückner, 2012).
55 Considering this, we investigated the role of these specialized hematopoietic pockets in hemocyte
56 transdifferentiation.

57

58 **Results**

59 *Phagocytic plasmatocytes transdifferentiate to crystal cells*

60 First we examined the formation of crystal cells and their anatomical locations during larval
61 development. We quantified crystal cells using a traditional way of labeling crystal cells based on
62 their expression of prophenoloxidases (Corcoran and Brückner, 2020; Rizki and Rizki, 1959),
63 enzymes responsible for melanization, the main immune function of crystal cells (Bidla et al., 2009;
64 Dudzic et al., 2015; Lu et al., 2014). Induction of melanization blackens crystal cells (Corcoran and
65 Brückner, 2020; Rizki and Rizki, 1959) and marks similar cell populations as the crystal cell reporter
66 *lozenge-GAL4* (*lz-GAL4; UAS-GFP*) (SupplFig. 1 A, B). During larval development, crystal cell
67 numbers increase slowly over the first and second larval instar stages, but expand more rapidly
68 during the third instar stage (Fig. 1 A), largely mirroring the exponential increase of plasmatocytes
69 during larval development (Fig 1 B) (Makhijani et al., 2011; Petraki et al., 2015). To visualize the
70 locations of crystal cells and plasmatocytes, we coexpressed two fluorescent protein reporters (for
71 crystal cells *BcF2-GFP* (Tokusumi et al., 2009), and for plasmatocytes *Hml*Δ*-DsRed* (Makhijani et
72 al., 2011)). Interestingly, crystal cells are strongly enriched in a cluster in the terminal segment of the
73 *Drosophila* larva, a region where plasmatocytes are also known to accumulate (Fig. 1 C-C'', D-D')
74 (Makhijani et al., 2011). Crystal cells are occasionally also found in other hematopoietic pockets, and
75 in dorsal vessel-associated clusters where floating hemocytes accumulate (Cevik et al., 2019; Petraki
76 et al., 2015).

77 Since previous studies suggested plasmatocyte-to-crystal cell transdifferentiation solely based on live
78 imaging (Leitao and Sucena, 2015), we sought an independent functional lineage tracing approach.
79 Asking whether crystal cells derive from undifferentiated progenitors or differentiated,
80 phagocytically active plasmatocytes, we traced cells based on the unique ability of differentiated
81 plasmatocytes to phagocytically uptake fluorescently labeled beads (Fig. 1 E-E'''). We injected
82 *Drosophila* larvae expressing fluorescent reporters for plasmatocytes and crystal cells with blue

83 fluorescent latex beads. Injected larvae were incubated in a time course, followed by the release of
84 hemocytes and quantification of the relative fractions of phagocytosis-labeled plasmatocytes and -
85 crystal cells (Fig. 1 F, G). The fraction of blue bead positive plasmatocytes quickly reached saturation
86 (~50% at 1h, ~90% at 4h and 22h). In contrast, crystal cells were labeled by blue beads with a
87 significant time delay (<10% at 1h, ~ 50% at 4h, ~70% at 22h) (Fig. 1 G). Together with previous
88 reports that suggested crystal cells are not capable of phagocytosis or proliferation (Lanot et al., 2001;
89 Leitao and Sucena, 2015; Tattikota et al., 2019) this supports a model of plasmatocyte-to-crystal cell
90 transdifferentiation, in which crystal cells derive from phagocytically active plasmatocyes, rather than
91 from undifferentiated, phagocytosis-incompetent progenitors.

92 *Sensory neuron activity promotes crystal cell transdifferentiation*

93 Next, we investigated the anatomical locations of crystal cells and plasmatocytes relative to sensory
94 neurons, using fluorescent reporters and live imaging, including the sensory neuron specific driver
95 *21-7-GAL4, UAS-CD8-GFP* (Song et al., 2007) (Fig. 2 A). We found that both plasmatocytes and
96 crystal cells colocalize with sensory neurons, with one important difference: plasmatocytes are found
97 in all hematopoietic pockets (Fig. 2 A), while crystal cells are mainly localized in the terminal
98 hematopoietic pocket of the larva (Fig. 2 B).

99 Given this colocalization with sensory neurons, we asked whether sensory neuron activity has an
100 effect on crystal cell generation. To mimic activation of sensory neurons, we exposed larvae to the
101 acetylcholine receptor agonist carbamoycholine (carbachol). Carbachol exposure over 4 hours
102 resulted in a moderate increase of crystal cell numbers (Fig. 2 C). More specifically and
103 complementary to this, we silenced sensory neurons by transient expression of *Kir2.1*, an inward
104 rectifying K+ channel that causes neuron hyperpolarization (Baines et al., 2001). Interestingly, *Kir2.1*
105 expression over 22 hours caused a dramatic drop in crystal cell numbers (Fig. 2 D). There was no
106 significant effect of neuronal silencing on total hemocyte numbers under comparable conditions
107 (SupplFig. 2 and (Makhijani et al., 2017)). To address whether sensory neuron silencing by Kir2.1
108 affects plasmatocyte to crystal cell transdifferentiation, we performed phagocytosis lineage tracing.
109 Indeed, transient neuronal silencing affects the fraction of crystal cells derived from blue bead labeled
110 plasmatocytes, while the ability of plasmatocytes to phagocytose remains the same (Fig. 2 E, F).
111 Taken together, our findings suggest that sensory neuron activity promotes transdifferentiation of
112 plasmatocytes to crystal cells.

113

114 *Crystal cells colocalize with, and require, sensory neurons of the sensory cones*

115 To gain more insight, we focused on the caudal cluster of crystal cells. Closer inspection of combined
116 fluorescent reporters for crystal cells and sensory neurons showed that crystal cells colocalize
117 particularly well with sensory organs of the sensory cones (Fig. 3 A-A'' and C-D''), protruding
118 structures that are grouped around the posterior spiracles, the terminal tubes of the tracheal system
119 (Hayashi and Kondo, 2018; Kuhn et al., 1992). Plasmatocytes accumulate in a large cluster around
120 the sensory cones already in the 2nd instar larva (Fig. 3 B-B''), which seems to foreshadow the pattern
121 and abundance of crystal cells in the 3rd instar larva (Fig. 3 D-D''). We therefore hypothesized that
122 many plasmatocytes of the 2nd instar larva may transdifferentiate to crystal cells, as is apparent in the
123 3rd instar.

124 Given the intriguing colocalization of crystal cells and sensory neurons and the dependence of blood
125 cell transdifferentiation on neuronal activity, we investigated the specific requirement of sensory cone
126 neurons for crystal cell production. A group of genes specifically expressed in sensory cone neurons
127 are atypical guanylyl cyclases, *Gyc88E*, *Gyc89Da*, and *Gyc89Db* (Vermehren-Schmaedick et al.,
128 2010). Using the driver *Gyc89Db-GAL4* (Vermehren-Schmaedick et al., 2010) (Fig. 3 E, F), we
129 ablated sensory cone neurons by expressing the proapoptotic gene *head involution defect (Hid)* in its
130 non-repressible version (*Hid* ^{ala5}) (Bergmann et al., 2002). Ablation of sensory cone neurons did not
131 affect larval viability, but it strongly reduced crystal cell numbers (Fig. 3 G). Conversely, ectopic
132 activation of sensory cone neurons by specific expression and transient induction of the heat-induced
133 cation channel TrpA1 (Hamada et al., 2008) caused a significant increase in crystal cells (Fig. 3 H).
134 Taken together, we conclude that crystal cells and their precursor plasmatocytes are strongly enriched
135 at the sensory cones of the larva. Sensory cone neurons, and their activity, are required for crystal
136 cells.

137 *Oxygen sensing through atypical guanylyl cyclases drives plasmatocyte-to-crystal cell*
138 *transdifferentiation*

139 The atypical guanylyl cyclases Gyc88E, Gyc89Da, and Gyc89Db are cytoplasmic oxygen sensors
140 that form heterodimers of Gyc88E and either Gyc89Da or Gyc89Db, and Gyc88E homodimers
141 (Huang et al., 2007; Morton, 2004; Morton et al., 2005; Vermehren et al., 2006). Activated Gyc
142 complexes generate the second messenger cyclic GMP (cGMP), which in turn activates neurons
143 (Morton, 2004; Morton et al., 2008). Since we found that sensory cone neurons expressing these
144 genes are required for crystal cell formation, we decided to test Gyc function itself in relation to

145 crystal cell transdifferentiation. When the obligatory subunit, Gyc88E, was silenced in the sensory
146 cone neurons, crystal cell numbers were reduced (Fig. 4 A). Phagocytosis lineage tracing confirmed
147 that Gyc function is required for transdifferentiation of plasmatocytes to crystal cells, as the fraction
148 of crystal cells carrying blue beads was significantly reduced in *Gyc88E* RNAi knockdowns, while
149 phagocytosis by plasmatocytes remained the same (Fig. 4 B). Given the role of Gycs as oxygen
150 sensors, we next investigated the effect of varying atmospheric oxygen concentrations on crystal cell
151 formation. Assessing crystal cell numbers per larva as readout, we exposed larvae to 8% or 5%
152 oxygen for 6 hours. Compared to normoxia (~21% oxygen), 8% hypoxia caused mild reduction in
153 crystal cells and 5% oxygen caused a significant drop in crystal cells, while total hemocyte numbers
154 stayed constant (SupplFig. 3 A, B, Fig. 4 C). Following up on the robust results obtained under 5%
155 oxygen, we determined whether hypoxia affects blood cell transdifferentiation, performing
156 phagocytosis lineage tracing for 6 hours under hypoxic conditions (5% O_2) and normoxia.
157 Interestingly, hypoxia phenocopies silencing of Gyc function in sensory cone neurons, resulting in a
158 significant reduction of blue beads in crystal cells, while phagocytosis levels of plasmatocytes remain
159 unaffected (Fig. 4 D). We therefore conclude that oxygen sensing through atypical guanylyl cyclases
160 (Gycs) that are linked to activation of the sensory cone neurons drives plasmatocyte-to-crystal cell
161 transdifferentiation (Fig. 4 E). This model supports the kinetics of crystal cells following
162 plasmatocyte expansion, based on the transition of plasmatocytes to crystal cells in particular in the
163 proximity of sensory cone neurons (SupplFig. 4 A).

164

165 **Discussion**

166 Our work has identified an unexpected mechanistic link between oxygen sensing and blood cell
167 transdifferentiation, which is facilitated through a particular set of sensory neurons and intracellular
168 Gyc oxygen sensors. This new paradigm inspires the search for similar principles of neuronally
169 controlled blood cell transdifferentiation that responds to environmental conditions in other species
170 including humans.

171 Transdifferentiation results in the conversion of one differentiated cell type to another. In some
172 systems, new differentiated cell types arise after de-differentiation to a transient pluripotent
173 intermediate (Graf, 2011; Pesaresi et al., 2019; Reid and Tursun, 2018). Our work supports a model
174 of direct transdifferentiation based on fluorescent reporters and phagocytosis lineage tracing.
175 Independent approaches also support a model of continuous blood cell transdifferentiation from

176 plasmatocytes to crystal cells through progressive states, based on single cell RNAseq pseudotime
177 lineage analysis (Tattikota et al., 2019). Transdifferentiation may be the fastest and most efficient
178 way for animals to shape the composition of their blood cell pool according to environmental
179 conditions such as oxygen levels and potentially other inputs.

180 Gyc intracellular oxygen sensors mediate oxygen detection in sensory neurons (Vermehren et al.,
181 2006), similar to other oxygen sensing mechanisms known in vertebrate neurons and other sensory
182 cells (Caravagna and Seaborn, 2016; Pokorski et al., 2016). In contrast, HIF (hypoxia inducible
183 factor) transcription factors regulate target genes in response to low oxygen conditions in a variety of
184 cell types (Gorr et al., 2006; Majmundar et al., 2010). Hypoxia, through HIF, regulates mammalian
185 hematopoiesis, lymphopoiesis and erythropoiesis (Chabi et al., 2019; Haase, 2013; Imanirad and
186 Dzierzak, 2013). The *Drosophila* HIF1a *sima* (*similar*) plays a role in crystal cell formation in the
187 *Drosophila* lymph gland (Mukherjee et al., 2011), however this effect is independent of HIF1β and
188 hypoxia target genes. Instead, formation of *Drosophila* crystal cells has been linked to Notch
189 signaling at various developmental stages (Duvic et al., 2002; Krzemien et al., 2007; Lebestky et al.,
190 2000; Lebestky et al., 2003; Leitao and Sucena, 2015; Mukherjee et al., 2011). It remains to be
191 determined whether oxygen sensing neurons and/or the signal receiving plasmatocytes are connected
192 to Notch signaling or an independent pathway that governs the fate switch of plasmatocytes to crystal
193 cells.

194 Linking oxygen sensing to crystal cell formation via Gycs may have several advantages. (1) Oxygen
195 sensing by neurons is more sensitive and immediate, and respond to a variety of environmental
196 conditions. Sensory cone neurons are at all times in contact with the surrounding atmosphere, based
197 on social burying behaviors during feeding, when larvae expose their caudal ends with the sensory
198 cones, also allowing air intake to the tracheal system through the neighboring posterior spiracles
199 (Hayashi and Kondo, 2018; Wu et al., 2003) (SupplFig. 4 B); eventually larvae exit the food source
200 to pupariate (Wu et al., 2003) (SupplFig. 4 B). With their exposed nature, the sensory neurons may
201 also integrate other inputs such as chemical cues or even light from the environment (Stewart et al.,
202 2015; Vermehren-Schmaedick et al., 2011; Xiang et al., 2010) when communicating to their targets.
203 (2) Activation of the sensory cone neurons coordinates blood cell transdifferentiation with other
204 responses to hypoxia, such as a behavioral escape response to hypoxic conditions (Morton, 2011;
205 Vermehren-Schmaedick et al., 2010). In this context, Gycs generate cGMP, which activates cyclic
206 nucleotide gated channels (CNG) (Morton et al., 2008; Vermehren-Schmaedick et al., 2010). CNG

207 channels mediate influx of calcium ions, resulting in consecutive activation of calmodulin/CaMK
208 signaling and sensory transduction (Kaupp and Seifert, 2002; Pifferi et al., 2006).

209 Neuronal regulation of the hematopoietic system and other organs is an important paradigm in
210 biology, which is starting to come to light in a variety of species (Kumar and Brockes, 2012). In
211 *Drosophila,* neuronal regulation of hematopoiesis is well established. Embryonic-lineage
212 plasmatocytes depend on sensory neurons for their survival, proliferation and localization (Gold and
213 Brückner, 2014, 2015; Makhijani et al., 2017; Makhijani et al., 2011; Makhijani and Brückner, 2012).
214 Activin-β, a TGF-β family ligand, is a key signal produced by active sensory neurons that promotes
215 plasmatocyte proliferation and adhesion (Makhijani et al., 2017). Identification of the signal/s from
216 active sensory cone neurons that trigger transdifferentiation will be the focus of intense future study.
217 We postulate secreted factor/s, which could potentially, albeit at reduced efficiency, also act at a
218 distance, promoting transdifferentiation of smaller numbers of crystal cells in the dorsal vessel
219 associated hemocyte clusters (Leitao and Sucena, 2015) and segmental hematopoietic pockets. In this
220 context it is interesting to note that in long term memory formation, Activin expression is induced
221 downstream of calmodulin/CaMK/CREB signaling in both *Drosophila* and vertebrates (Inokuchi et
222 al., 1996; Miyashita et al., 2012), suggesting potential parallels of this signaling cassette in neuron-
223 induced blood cell transdifferentiation.

224 In vertebrates, functional links of hematopoiesis with sensory neurons or other sensing systems
225 remain largely unknown, despite some aspects of bone marrow hematopoiesis and inflammatory
226 responses being regulated by the autonomic nervous system (Hanoun et al., 2015; Pavlov and Tracey,
227 2012). Oxygen sensing could be an important regulatory factor in recently identified hematopoietic
228 sites such as the vertebrate lung, which provides a microenvironment for limited blood cell
229 progenitors and megakaryocytes that are active in platelet production (Lefrancais et al., 2017; Martin
230 et al., 1983). The lung, like many other organs, also harbors tissue macrophages that proliferate in
231 local microenvironments and bear evolutionary parallels with *Drosophila* embryonic-lineage
232 plasmatocytes (Gold and Brückner, 2014, 2015; Perdiguero and Geissmann, 2016). Interestingly, the
233 lung and airways are rich in vagal afferent nerves that sense chemical and mechanical cues (Chang et
234 al., 2015; Mazzone and Undem, 2016), and neuroendocrine cells of the lung that sense oxygen early
235 in life and later provide a microenvironment for airway epithelial cells (Caravagna and Seaborn,
236 2016; Cutz et al., 2007). Investigation of sensory neurons and other sensors may therefore open a new
237 chapter in the regulation of vertebrate hematopoiesis, transdifferentiation, and immune cell fate and
238 function.

Materials and Methods

Drosophila Strains

Drosophila drivers, reporters and related lines used were *HmlΔ-GAL4, UAS-GFP* (Sinenko and Mathey-Prevot, 2004)*;* combination driver *HmlΔGAL4, UAS-GFP; He-GAL4* ((Yang et al., 2015) gift from Dan Hultmark), *lz-GAL4; UAS-GFP* (J. Pollock, Bloomington), *21-7-GAL4* (Makhijani et al., 2011; Song et al., 2007) *Gyc89Db-GAL4 (Morton et al., 2008); BcF6-GFP* (Tokusumi et al., 2009), *BcF6-mCherry* (Tokusumi et al., 2009), *BcF2-GFP* (Tokusumi et al., 2009); *HmlΔ-DsRed* (Makhijani et al., 2011); and *tubGAL80ts* (McGuire et al., 2003). UAS lines used were *UAS-CD8-GFP* (Song et al., 2007); *UAS-Kir2.1* (Baines et al., 2001) (Bloomington); *UAS-TrpA1* (Bloomington); *UAS-Hid ala5* (Bergmann et al., 2002); *UAS-Gyc88E RNAi* (Bloomington). Control lines used were *w1118* (Bloomington) or *yw* (Bloomington). Unless otherwise stated, fly crosses were set and maintained at 25° Celsius. Crosses with the driver *Gyc89Db-GAL4* were performed at 29°C to enhance expression.

Hemocyte Quantification

Total hemocyte quantification was performed essentially as described in (Corcoran and Brückner, 2020; Petraki et al., 2015). All fluorescently-marked hemocytes of single larvae were released into wells marked by a hydrophobic PAP pen (Beckman Coulter) on glass slides filled with 20-30 µL PBS. Cells were allowed to settle for 15-20 min, and were imaged by fluorescence tile scan microscopy on a Leica DMI4000B microscope with Leica DFC350FX camera and 20x objective. Cell numbers in images were analyzed by particle quantification using Fiji/ImageJ (Corcoran and Brückner, 2020; Petraki et al., 2015; Schindelin et al., 2012).

Crystal cell quantification was performed using fluorescent protein reporters or melanization. To quantify crystal cells in live animals, larvae were placed on a slide in a small drop of 10-15 µl PBS with a coverslip on top. Fluorescent crystal cells in each segment were manually counted, rolling the larva by gently moving the coverslip. For phagocytosis lineage tracing, fluorescent crystal cells were quantified ex vivo (see below). To quantify crystal cells based on their ability to melanize (due to their hallmark expression of functional Prophenoloxidase 1 and 2) larvae were placed in 250 µl of PBS in Eppendorf tubes and heated at 65° Celsius for 22 minutes in a heat block, and melanized (black) cells were quantified under a stereoscope by manual counting (Corcoran and Brückner, 2020; Rizki and Rizki, 1959).

269 Larvae were analyzed at various developmental times after egg laying (AEL) corresponding to the
270 following size ranges: 1st instar: ~0.5-1.4mm (22-46h AEL; 2nd instar: ~1.5-2.6mm (47-77h AEL); 3rd
271 instar: ~2.7- >3.5mm (from 78h AEL). For the crosses used, no developmental delays were observed;
272 therefore selection of specified larval size ranges from 24h embryo collections was used in lieu of
273 more tightly timed embryo collections.

274 *Manipulation of Neuronal Activity*

275 To mimic sensory neuron stimulation, larvae were exposed to 10mg/ml carbamylcholine (carbachol,
276 Sigma Aldrich) in fly food for 4 hours allowing direct cuticle contact with carbachol (Makhijani et
277 al., 2017).

278 To activate specific neuron populations, the heat-inducible cation channel TrpA1 was ectopically
279 expressed and transiently heat induced to mimic neuron activation (Hamada et al., 2008).
280 Sopecifically, *TrpA1* crosses were set at RT and shifted to 29°C for 4h. Larvae were analyzed within
281 30 minutes following this period.

282 Sensory neuron silencing was achieved by transiently expressing a transgenic of the inward rectifying
283 potassium channel Kir2.1 (Baines et al., 2001), under control of a sensory neuron specific GAL4
284 driver and a temperature-sensitive GAL4 inhibitor GAL80ts (McGuire et al., 2003); genotypes for
285 neuronal silencing experiments were *21-7-GAL4, UAS-GFP, HmlΔDsRed/UAS-Kir2.1;*
286 *tubGAL80ts/+* with controls *21-7-GAL4, UAS-GFP, HmlΔDsRed/+; tubGAL80ts/+*. F1 from crosses
287 were raised at 18° Celsius. To temporarily silence sensory neurons, larvae were shifted from 18° to
288 29° Celsius for 22 hours to destabilize GAL80ts, allowing for expression of Kir2.1, which
289 hyperpolarizes sensory neuron preventing firing. Larvae were analyzed within 1 hour post-silencing.

290 *Phagocytosis Lineage Tracing*

291 For lineage tracing of crystal cells that derive from actively phagocytic plasmatocytes, larvae with
292 genotype *HmlΔGAL4, UAS-GFP; BcF6-mCherry* were injected with 69 nl of blue fluorescent
293 FluoSphere Carboxylate-modified 0.2 um beads (Invitrogen) diluted 1:100 in PBS using a Nanoject
294 injector (Drummond Scientific). After injection, larvae were placed on food with yeast for 4 hours.
295 Hemocytes of individual larvae were then released into a well marked on a glass slide by PAP pen
296 and filled with 20-30 µl PBS; hemocytes were allowed to settle for 15-20 minutes in a wet chamber
297 (Corcoran and Brückner, 2020; Petraki et al., 2015). Cells were imaged with a Leica DMI4000
298 microscope with tilescan function. Cell quantification was conducted manually from a representative

central field of each image (containing ~150-300 plasmatocytes). For genotypes that give rise to substantially reduced numbers of crystal cells, crystal cells of the whole tilescan area were analyzed. Transdifferentiation was quantified by comparing ratios of crystal cells positive for blue particles/ total crystal cells (mCherry positive) for various experimental and control conditions. The same quantification for plasmatocytes (GFP positive) with blue beads relative to all plasmatocytes was conducted as an internal control for injection efficiency and phagocytic fitness.

Hypoxia experiments

Hypoxia experiments were conducted using a hypoxic chamber (Biospherix, Inc., Laconia, NY). Oxygen concentrations were set as indicated, supplementing reduced O_2 with N_2. Incubations were performed at room temperature (RT) for 6h. Crystal cell melanization assays were conducted with larvae of the genotype w^{1118}, and phagocytic lineage tracing and total hemocyte experiments used *Hml*Δ*-GAL4, UAS-GFP; BcF6-mCherry* larvae. For all experiments, 15-25 larvae of the desired age/size and genotype were placed on inactivated yeast paste in cell strainer snap cap tubes, allowing for rapid gas exchange (Corning #352235). Six cell strainer tubes were held by a fitted rack that was inserted into a large cylindrical polystyrene *Drosophila* population cage with steel mesh on one side (custom construction). During transport from the hypoxic chamber to the bench, population cages were sealed in a plastic bag to maintain hypoxic conditions up to the point when larvae were analyzed. Control samples were placed in an identical setup but left at normoxic conditions at comparable temperature (RT) and time (6h). Following hypoxia/normoxia conditions, assays were conducted as described in the respective paragraphs.

Microscopy

Released hemocytes were imaged on a Leica DMI4000B microscope as described above. Live imaging of larvae was done as described previously, immobilizing larvae on an ice-cooled metal block (Makhijani et al. *Development* 2011). Imaging was performed using a Leica M205FA fluorescent stereoscope with DFC300FX color digital camera and Leica LAS Montage module, combining z-stacks into single in-focus images.

Statistical Analysis

For all experiments numbers of larvae per genotype and condition are indicated in the Figure Legends. For each genotype and condition the mean and standard deviation were determined and significance was tested by 2-way ANOVA (Prism). For hemocyte counts over the course of larval

development, regression analysis was performed (Excel). For phagocytosis lineage tracing, the mean and standard deviation of percentages of blue bead positive cells were determined and assessed by 2-way ANOVA (Prism). P-value cutoffs for significance were as follows: * = $p < 0.05$, ** = $p < 0.01$, and *** = $p < 0.001$. Pools of both male and female larvae were analyzed.

Authors' contributions

KB conceived and supervised the study. SC, AM and KB planned the experiments. SC, AM, JA, YH, DO, TJ, KK carried out the experiments. SC, AM, JA, YH, DO, TJ, KK and KB analyzed the data. KB wrote the manuscript with input from all authors.

Competing interests

The authors have no competing interests.

Funding

This work was supported by grants from the American Cancer Society RSG DDC-122595, American Heart Association 13BGIA13730001, National Science Foundation 1326268, and National Institutes of Health 1R01GM112083, 1R56HL118726 and 1R01GM131094 (to KB).

Acknowledgements

We thank D. Morton, R. Schulz, U. Banerjee, A. Bergmann, C. Evans, D. Hultmark, Y.N. Jan, L. Kockel, the Bloomington Stock Center, and TRiP for fly stocks. We are grateful to Khalida Sabeur and Manideep Chavali for help to access and use hypoxia chamber equipment. Thanks to Ava Brückner-Kockel for advice on regression analysis. We thank members of the Brückner lab for discussion and feedback on the manuscript.

357 **References**

358

359 Baines, R.A., Uhler, J.P., Thompson, A., Sweeney, S.T., and Bate, M. (2001). Altered electrical
360 properties in *Drosophila* neurons developing without synaptic transmission. J Neurosci *21*, 1523-
361 1531.

362 Banerjee, U., Girard, J.R., Goins, L.M., and Spratford, C.M. (2019). *Drosophila* as a Genetic Model
363 for Hematopoiesis. Genetics *211*, 367-417.

364 Bergmann, A., Tugentman, M., Shilo, B.Z., and Steller, H. (2002). Regulation of cell number by
365 MAPK-dependent control of apoptosis: a mechanism for trophic survival signaling. Dev Cell *2*, 159-
366 170.

367 Bidla, G., Hauling, T., Dushay, M.S., and Theopold, U. (2009). Activation of insect phenoloxidase
368 after injury: endogenous versus foreign elicitors. J Innate Immun *1*, 301-308.

369 Caravagna, C., and Seaborn, T. (2016). Oxygen Sensing in Early Life. Lung *194*, 715-722.

370 Cevik, D., Acker, M., Michalski, C., and Jacobs, J.R. (2019). Pericardin, a *Drosophila* collagen,
371 facilitates accumulation of hemocytes at the heart. Dev Biol *454*, 52-65.

372 Chabi, S., Uzan, B., Naguibneva, I., Rucci, J., Fahy, L., Calvo, J., Arcangeli, M.L., Mazurier, F.,
373 Pflumio, F., and Haddad, R. (2019). Hypoxia Regulates Lymphoid Development of Human
374 Hematopoietic Progenitors. Cell Rep *29*, 2307-2320 e2306.

375 Chang, R.B., Strochlic, D.E., Williams, E.K., Umans, B.D., and Liberles, S.D. (2015). Vagal Sensory
376 Neuron Subtypes that Differentially Control Breathing. Cell *161*, 622-633.

377 Cieslar-Pobuda, A., Knoflach, V., Ringh, M.V., Stark, J., Likus, W., Siemianowicz, K., Ghavami, S.,
378 Hudecki, A., Green, J.L., and Los, M.J. (2017). Transdifferentiation and reprogramming: Overview
379 of the processes, their similarities and differences. Biochim Biophys Acta Mol Cell Res *1864*, 1359-
380 1369.

381 Cirovic, B., Schonheit, J., Kowenz-Leutz, E., Ivanovska, J., Klement, C., Pronina, N., Begay, V., and
382 Leutz, A. (2017). C/EBP-Induced Transdifferentiation Reveals Granulocyte-Macrophage Precursor-
383 like Plasticity of B Cells. Stem Cell Reports *8*, 346-359.

384 Collombet, S., van Oevelen, C., Sardina Ortega, J.L., Abou-Jaoude, W., Di Stefano, B., Thomas-
385 Chollier, M., Graf, T., and Thieffry, D. (2017). Logical modeling of lymphoid and myeloid cell
386 specification and transdifferentiation. Proc Natl Acad Sci U S A *114*, 5792-5799.

387 Corcoran, S., and Brückner, K. (2020). Quantification of blood cells in *Drosophila* and other insects.
388 Springer Protocols Handbooks: Immunity in Insects *Sandrelli F, Tettamanti G, editors*, 65-77.

389 Cutz, E., Yeger, H., and Pan, J. (2007). Pulmonary neuroendocrine cell system in pediatric lung
390 disease-recent advances. Pediatr Dev Pathol *10*, 419-435.

391 Davies, L.C., Jenkins, S.J., Allen, J.E., and Taylor, P.R. (2013). Tissue-resident macrophages. Nat
392 Immunol *14*, 986-995.

393 Di Tullio, A., Vu Manh, T.P., Schubert, A., Castellano, G., Mansson, R., and Graf, T. (2011).
394 CCAAT/enhancer binding protein alpha (C/EBP(alpha))-induced transdifferentiation of pre-B cells
395 into macrophages involves no overt retrodifferentiation. Proc Natl Acad Sci U S A *108*, 17016-
396 17021.

397 Dudzic, J.P., Kondo, S., Ueda, R., Bergman, C.M., and Lemaitre, B. (2015). *Drosophila* innate
398 immunity: regional and functional specialization of prophenoloxidases. BMC Biol *13*, 81.

399 Duvic, B., Hoffmann, J.A., Meister, M., and Royet, J. (2002). Notch signaling controls lineage
400 specification during *Drosophila* larval hematopoiesis. Curr Biol *12*, 1923-1927.

401 Gold, K.S., and Brückner, K. (2014). *Drosophila* as a model for the two myeloid blood cell systems
402 in vertebrates. Exp Hematol *42*, 717-727.

403 Gold, K.S., and Brückner, K. (2015). Macrophages and cellular immunity in *Drosophila*
404 *melanogaster*. Semin Immunol *27*, 357-368.

405 Gorr, T.A., Gassmann, M., and Wappner, P. (2006). Sensing and responding to hypoxia via HIF in
406 model invertebrates. J Insect Physiol *52*, 349-364.

407 Graf, T. (2011). Historical origins of transdifferentiation and reprogramming. Cell Stem Cell *9*, 504-
408 516.

409 Haase, V.H. (2013). Regulation of erythropoiesis by hypoxia-inducible factors. Blood Rev *27*, 41-53.

410 Hamada, F.N., Rosenzweig, M., Kang, K., Pulver, S.R., Ghezzi, A., Jegla, T.J., and Garrity, P.A.
411 (2008). An internal thermal sensor controlling temperature preference in *Drosophila*. Nature *454*,
412 217-220.

413 Hanoun, M., Maryanovich, M., Arnal-Estape, A., and Frenette, P.S. (2015). Neural regulation of
414 hematopoiesis, inflammation, and cancer. Neuron *86*, 360-373.

415 Hayashi, S., and Kondo, T. (2018). Development and Function of the *Drosophila* Tracheal System.
416 Genetics *209*, 367-380.

417 Holz, A., Bossinger, B., Strasser, T., Janning, W., and Klapper, R. (2003). The two origins of
418 hemocytes in *Drosophila*. Development *130*, 4955-4962.

419 Huang, S.H., Rio, D.C., and Marletta, M.A. (2007). Ligand binding and inhibition of an oxygen-
420 sensitive soluble guanylate cyclase, Gyc-88E, from *Drosophila*. Biochemistry *46*, 15115-15122.

421 Imanirad, P., and Dzierzak, E. (2013). Hypoxia and HIFs in regulating the development of the
422 hematopoietic system. Blood Cells Mol Dis *51*, 256-263.

423 Inokuchi, K., Kato, A., Hiraia, K., Hishinuma, F., Inoue, M., and Ozawa, F. (1996). Increase in
424 activin beta A mRNA in rat hippocampus during long-term potentiation. FEBS Lett *382*, 48-52.

425 Kaupp, U.B., and Seifert, R. (2002). Cyclic nucleotide-gated ion channels. Physiol Rev *82*, 769-824.

426 Krzemien, J., Dubois, L., Makki, R., Meister, M., Vincent, A., and Crozatier, M. (2007). Control of
427 blood cell homeostasis in *Drosophila* larvae by the posterior signalling centre. Nature *446*, 325-328.

428 Kuhn, D.T., Sawyer, M., Packert, G., Turenchalk, G., Mack, J.A., Sprey, T.E., Gustavson, E., and
429 Kornberg, T.B. (1992). Development of the D. *melanogaster* caudal segments involves suppression
430 of the ventral regions of A8, A9 and A10. Development *116*, 11-20.

431 Kumar, A., and Brockes, J.P. (2012). Nerve dependence in tissue, organ, and appendage regeneration.
432 Trends in neurosciences *35*, 691-699.

433 Lanot, R., Zachary, D., Holder, F., and Meister, M. (2001). Postembryonic hematopoiesis in
434 *Drosophila*. Dev Biol *230*, 243-257.

435 Lebestky, T., Chang, T., Hartenstein, V., and Banerjee, U. (2000). Specification of *Drosophila*
436 hematopoietic lineage by conserved transcription factors. Science *288*, 146-149.

437 Lebestky, T., Jung, S.H., and Banerjee, U. (2003). A Serrate-expressing signaling center controls
438 *Drosophila* hematopoiesis. Genes Dev *17*, 348-353.

439 Lefrancais, E., Ortiz-Munoz, G., Caudrillier, A., Mallavia, B., Liu, F., Sayah, D.M., Thornton, E.E.,
440 Headley, M.B., David, T., Coughlin, S.R.*, et al.* (2017). The lung is a site of platelet biogenesis and a
441 reservoir for haematopoietic progenitors. Nature *544*, 105-109.

442 Leitao, A.B., and Sucena, E. (2015). *Drosophila* sessile hemocyte clusters are true hematopoietic
443 tissues that regulate larval blood cell differentiation. Elife *4*.

444 Li, P., Burke, S., Wang, J., Chen, X., Ortiz, M., Lee, S.C., Lu, D., Campos, L., Goulding, D., Ng,
445 B.L.*, et al.* (2010). Reprogramming of T cells to natural killer-like cells upon Bcl11b deletion.
446 Science *329*, 85-89.

447 Lu, A., Zhang, Q., Zhang, J., Yang, B., Wu, K., Xie, W., Luan, Y.X., and Ling, E. (2014). Insect
448 prophenoloxidase: the view beyond immunity. Front Physiol *5*, 252.

449 Majmundar, A.J., Wong, W.J., and Simon, M.C. (2010). Hypoxia-inducible factors and the response
450 to hypoxic stress. Mol Cell *40*, 294-309.

451 Makhijani, K., Alexander, B., Rao, D., Petraki, S., Herboso, L., Kukar, K., Batool, I., Wachner, S.,
452 Gold, K.S., Wong, C.*, et al.* (2017). Regulation of *Drosophila* hematopoietic sites by Activin-beta
453 from active sensory neurons. Nat Commun *8*, 15990.

454 Makhijani, K., Alexander, B., Tanaka, T., Rulifson, E., and Brückner, K. (2011). The peripheral
455 nervous system supports blood cell homing and survival in the *Drosophila* larva. Development *138*,
456 5379-5391.

457 Makhijani, K., and Brückner, K. (2012). Of blood cells and the nervous system: Hematopoiesis in the
458 *Drosophila* larva. Fly (Austin) *6*, 254-260.

459 Markus, R., Laurinyecz, B., Kurucz, E., Honti, V., Bajusz, I., Sipos, B., Somogyi, K., Kronhamn, J.,
460 Hultmark, D., and Ando, I. (2009). Sessile hemocytes as a hematopoietic compartment in *Drosophila*
461 *melanogaster*. Proc Natl Acad Sci U S A *106*, 4805-4809.

462 Martin, J.F., Slater, D.N., and Trowbridge, E.A. (1983). Abnormal intrapulmonary platelet
463 production: a possible cause of vascular and lung disease. Lancet *1*, 793-796.

464 Mazzone, S.B., and Undem, B.J. (2016). Vagal Afferent Innervation of the Airways in Health and
465 Disease. Physiol Rev *96*, 975-1024.

466 McGuire, S.E., Le, P.T., Osborn, A.J., Matsumoto, K., and Davis, R.L. (2003). Spatiotemporal rescue
467 of memory dysfunction in *Drosophila*. Science *302*, 1765-1768.

468 Miyashita, T., Oda, Y., Horiuchi, J., Yin, J.C., Morimoto, T., and Saitoe, M. (2012). Mg(2+) block of
469 *Drosophila* NMDA receptors is required for long-term memory formation and CREB-dependent gene
470 expression. Neuron *74*, 887-898.

471 Morton, D.B. (2004). Atypical soluble guanylyl cyclases in *Drosophila* can function as molecular
472 oxygen sensors. J Biol Chem *279*, 50651-50653.

473 Morton, D.B. (2011). Behavioral responses to hypoxia and hyperoxia in *Drosophila* larvae:
474 molecular and neuronal sensors. Fly (Austin) *5*, 119-125.

475 Morton, D.B., Langlais, K.K., Stewart, J.A., and Vermehren, A. (2005). Comparison of the properties
476 of the five soluble guanylyl cyclase subunits in *Drosophila melanogaster*. J Insect Sci *5*, 12.

477 Morton, D.B., Stewart, J.A., Langlais, K.K., Clemens-Grisham, R.A., and Vermehren, A. (2008).
478 Synaptic transmission in neurons that express the *Drosophila* atypical soluble guanylyl cyclases,
479 Gyc-89Da and Gyc-89Db, is necessary for the successful completion of larval and adult ecdysis. J
480 Exp Biol *211*, 1645-1656.

481 Mukherjee, T., Kim, W.S., Mandal, L., and Banerjee, U. (2011). Interaction between Notch and Hif-
482 alpha in development and survival of *Drosophila* blood cells. Science *332*, 1210-1213.

483 Pavlov, V.A., and Tracey, K.J. (2012). The vagus nerve and the inflammatory reflex--linking
484 immunity and metabolism. Nature reviews. Endocrinology *8*, 743-754.

485 Perdiguero, E.G., and Geissmann, F. (2016). The development and maintenance of resident
486 macrophages. Nat Immunol *17*, 2-8.

487 Pesaresi, M., Sebastian-Perez, R., and Cosma, M.P. (2019). Dedifferentiation, transdifferentiation and
488 cell fusion: in vivo reprogramming strategies for regenerative medicine. Febs J *286*, 1074-1093.

489 Petraki, S., Alexander, B., and Brückner, K. (2015). Assaying Blood Cell Populations of the
490 *Drosophila melanogaster* Larva. J Vis Exp.

491 Pifferi, S., Boccaccio, A., and Menini, A. (2006). Cyclic nucleotide-gated ion channels in sensory
492 transduction. FEBS Lett *580*, 2853-2859.

493 Pokorski, M., Takeda, K., and Okada, Y. (2016). Oxygen Sensing Mechanisms: A Physiological
494 Penumbra. Adv Exp Med Biol *952*, 1-8.

495 Rapino, F., Robles, E.F., Richter-Larrea, J.A., Kallin, E.M., Martinez-Climent, J.A., and Graf, T.
496 (2013). C/EBPalpha induces highly efficient macrophage transdifferentiation of B lymphoma and
497 leukemia cell lines and impairs their tumorigenicity. Cell Rep *3*, 1153-1163.

498 Reid, A., and Tursun, B. (2018). Transdifferentiation: do transition states lie on the path of
499 development? Curr Opin Syst Biol *11*, 18-23.

500 Rizki, M.T., and Rizki, R.M. (1959). Functional significance of the crystal cells in the larva of
501 *Drosophila melanogaster*. J Biophys Biochem Cytol *5*, 235-240.

502 Schindelin, J., Arganda-Carreras, I., Frise, E., Kaynig, V., Longair, M., Pietzsch, T., Preibisch, S.,
503 Rueden, C., Saalfeld, S., Schmid, B.*, et al.* (2012). Fiji: an open-source platform for biological-image
504 analysis. Nat Methods *9*, 676-682.

505 Sieweke, M.H., and Allen, J.E. (2013). Beyond stem cells: self-renewal of differentiated
506 macrophages. Science *342*, 1242974.

507 Sinenko, S.A., and Mathey-Prevot, B. (2004). Increased expression of *Drosophila* tetraspanin,
508 Tsp68C, suppresses the abnormal proliferation of ytr-deficient and Ras/Raf-activated hemocytes.
509 Oncogene *23*, 9120-9128.

510 Siripin, D., Kheolamai, P., Y, U.P., Supokawej, A., Wattanapanitch, M., Klincumhom, N.,
511 Laowtammathron, C., and Issaragrisil, S. (2015). Transdifferentiation of erythroblasts to
512 megakaryocytes using FLI1 and ERG transcription factors. Thromb Haemost *114*, 593-602.

513 Song, W., Onishi, M., Jan, L.Y., and Jan, Y.N. (2007). Peripheral multidendritic sensory neurons are
514 necessary for rhythmic locomotion behavior in *Drosophila* larvae. Proc Natl Acad Sci U S A *104*,
515 5199-5204.

516 Stewart, S., Koh, T.W., Ghosh, A.C., and Carlson, J.R. (2015). Candidate ionotropic taste receptors
517 in the *Drosophila* larva. Proc Natl Acad Sci U S A *112*, 4195-4201.

518 Tattikota, S.G., Hu, Y., Liu, Y., Cho, B., Barrera, V., Steinbaugh, M., Yoon, S.-H., Comjean, A., Li,
519 F., Dervis, F., *et al.* (2019). A single-cell survey of *Drosophila* blood. bioRxiv,
520 2019.2012.2020.884999.

521 Tokusumi, T., Shoue, D.A., Tokusumi, Y., Stoller, J.R., and Schulz, R.A. (2009). New hemocyte-
522 specific enhancer-reporter transgenes for the analysis of hematopoiesis in *Drosophila*. Genesis *47*,
523 771-774.

524 Vermehren, A., Langlais, K.K., and Morton, D.B. (2006). Oxygen-sensitive guanylyl cyclases in
525 insects and their potential roles in oxygen detection and in feeding behaviors. J Insect Physiol *52*,
526 340-348.

527 Vermehren-Schmaedick, A., Ainsley, J.A., Johnson, W.A., Davies, S.A., and Morton, D.B. (2010).
528 Behavioral responses to hypoxia in *Drosophila* larvae are mediated by atypical soluble guanylyl
529 cyclases. Genetics *186*, 183-196.

530 Vermehren-Schmaedick, A., Scudder, C., Timmermans, W., and Morton, D.B. (2011). *Drosophila*
531 gustatory preference behaviors require the atypical soluble guanylyl cyclases. J Comp Physiol A
532 Neuroethol Sens Neural Behav Physiol *197*, 717-727.

533 Wu, Q., Wen, T., Lee, G., Park, J.H., Cai, H.N., and Shen, P. (2003). Developmental control of
534 foraging and social behavior by the *Drosophila* neuropeptide Y-like system. Neuron *39*, 147-161.

535 Xiang, Y., Yuan, Q., Vogt, N., Looger, L.L., Jan, L.Y., and Jan, Y.N. (2010). Light-avoidance-
536 mediating photoreceptors tile the *Drosophila* larval body wall. Nature *468*, 921-926.

537 Xie, H., Ye, M., Feng, R., and Graf, T. (2004). Stepwise reprogramming of B cells into macrophages.
538 Cell *117*, 663-676.

539 Yang, H., Kronhamn, J., Ekstrom, J.O., Korkut, G.G., and Hultmark, D. (2015). JAK/STAT signaling
540 in *Drosophila* muscles controls the cellular immune response against parasitoid infection. EMBO
541 Rep *16*, 1664-1672.

542

543

544 **Figure Legends**

545

546 **Figure 1. Crystal cells in the *Drosophila* larva are generated by transdifferentiation**

547 (A) Development of crystal cell numbers over time. Crystal cells per larva, assessed by melanization,
548 relative to larval size and developmental stage. Genotype is w^{1118}, n=155. Mean and standard
549 deviation, regression analysis.

550 (B) Development of total hemocyte numbers over time. Total hemocytes per larva, genotype is
551 *HmlΔGAL4, UAS-GFP; He-GAL4*; n=107. Mean and standard deviation, regression analysis.

552 (C-C'') Localization of plasmatocytes and crystal cells in the 3rd instar larva,; genotype is *BcF2-GFP/*
553 *Hml*Δ*-DsRed*; plasmatocytes labeled by *Hml*Δ*-DsRed* (red); crystal cells labeled by *BcF2-GFP*
554 (green); lateral view, posterior right.

555 (D-D') Model of distribution of plasmatocyte (red) and crystal cells (orange) in *Drosophila* larva,
556 relevant sensory neuron clusters of the hematopoietic pockets (green); lateral view, posterior right.

557 (E-E''') Scheme of phagocytosis lineage tracing assay. Blue fluorescent latex beads are injected into
558 early 3rd instar larvae, cells are released after indicated incubation times; fraction of cells containing
559 phagocytosed beads are determined. Possible outcomes are depicted with crystal cells in orange,
560 plasmatocytes in red, progenitors in grey.

561 (F) Sample image of analyzed cells; genotype *BcF2-GFP/ Hml*Δ*-DsRed*; crystal cells in green,
562 plasmatocytes in red; blue arrowheads indicate crystal cells with incorporated blue beads.

563 (G) Quantification of samples as in (G); fraction of plasmatocytes and crystal cells containing blue
564 beads at time 1h, 4, 22h after injection; n=21; mean and standard deviation.

565

566 **Figure 2. Sensory Neuron activity regulates transdifferentiation to crystal cells**

567 (A) Plasmatocytes colocalize with sensory neurons in all hematopoietic pockets; genotype *21-7-*
568 *GAL4, UAS-CD8-GFP, Hml*Δ*DsRed/CyO* ; lateral view, posterior right.

569 (B) Crystal cells also colocalize with sensory neurons but are mainly found in a cluster at the caudal
570 end of the larva; genotype *21-7-GAL4, UAS-CD8-GFP/+; BCF6-mCherry/+*; lateral view, posterior
571 right.

572 (C) Treatment of larvae with the AchR agonist carbachol to mimic sensory neuron activation,
573 treatment for 4h; genotype is *yw*; quantification of crystal cells by melanization; control n=65 (+45);
574 carbachol n=34 (+50). Individual value plot with mean and standard deviation, two-way ANOVA.

575 (D) Transient silencing of sensory neurons, quantification of crystal cells by melanization; genotypes
576 are experiment *21-7-GAL4, UAS-CD8GFP, Hml*Δ*-DsRed/ UAS-Kir2.1; tubGAL80ts/* + and control
577 *21-7-GAL4, UAS-CD8GFP, Hml*Δ*-DsRed/ +; tubGAL80ts/* +. Larvae induced at 29˚C for 22h. Mean
578 and standard deviation, two-way ANOVA.

579 (E, F) Phagocytosis lineage tracing, genotypes are experiment *21-7-GAL4, UAS-CD8GFP, Hml*Δ-
580 *DsRed/ UAS-Kir2.1; BcF6-GFP/ tubGAL80ts*, and control *21-7-GAL4, UAS-CD8GFP, Hml*Δ*-DsRed/*
581 *+; BcF6-GFP/ tubGAL80ts*.

582 (E) Sample image of analyzed cells, plasmatocytes (red), crystal cells (green), injected beads (blue).

583 (F) Quantification of samples as in (E); fraction of plasmatocytes and crystal cells containing blue
584 beads, experiment n=12 and control n=12. Mean and standard deviation, two-way ANOVA.

585

586 **Figure 3. Crystal cells are clustered around the sensory cones and are promoted by sensory**
587 **cone neurons**

588 (A-D) Localization of sensory neurons, plasmatocytes and crystal cells, caudal view of larvae; scale
589 bars 0.25mm.

590 (A) Sensory neurons (green), genotype *21-7-GAL4, UAS-CD8-GFP, Hml*Δ*-DsRed/CyO*; 3rd instar
591 larva.

592 (B) Plasmatocytes (green) and crystal cells (red), genotype *Hml*Δ*-GAL4, UAS-GFP; BcF6-mCherry*;
593 2nd instar larva.

594 (C) Crystal cells (red) and sensory neurons (green), genotype *21-7-GAL4, UAS-CD8-GFP/+; BcF6-*
595 *mCherry/*+; 2nd instar larva.

596 (D) Crystal cells (red) and sensory neurons (green), *21-7-GAL4, UAS-CD8-GFP/+; BcF6-*
597 *mCherry/*+; 3rd instar larva.

598 (A'-D') Models corresponding to (A-D), respectively, plasmatocytes red, crystal cells orange,
599 sensory neurons green; caudal view.

600 (A''-D'') Models, lateral view, corresponding to (A-C and A'-C'), respectively; lateral view.

601 (E) *Gyc89Db-GAL4* driver expressing GFP in sensory cone neurons (green), lateral view, genotype is
602 *UAS-GFP/+; Gyc89Db-GAL4/+*; lateral view, posterior right; scale bar 0.5mm.

603 (F) Larva as in (E), caudal view.

604 (G) Ablation of sensory cone neurons affects crystal cells; quantification of crystal cells per larva by
605 melanization. Genotypes are experiment *UAS-Hid ala5/+; Gyc89Db-GAL4/tubGAL80ts*, n=34 and
606 control *Gyc89Db-GAL4/tubGAL80ts*, n=34. Crosses were raised at 18˚C and temperature shifted to
607 29 ˚C for 16 h. Individual value plot with mean and standard deviation, two-way ANOVA.

608 (H) Transient activation of TrpA1 in sensory cone neurons; quantification of crystal cells per larva by
609 melanization. Genotypes are experiment *UAS-TrpA1/ +; Gyc89Db-GAL4, / +*, n=46, and control
610 *Gyc89Db-GAL4/+*, n=48*;* in addition, one experiment F1 cohort *UAS-TrpA1/ +; Gyc89Db-GAL4, /*
611 *+*, n=47, was maintained as uninduced control at RT. Crosses were raised at RT and temperature
612 shifted to 29˚C for 4 hours;. Individual value plot with mean and standard deviation, two-way
613 ANOVA.

614

615 **Figure 4. Oxygen sensing through Gycs in sensory cone neurons drives plasmatocyte-to-crystal**
616 **cell transdifferentiation**

617 (A) RNAi silencing of *Gyc88E* in sensory cone neurons results in reduced crystal cell numbers
618 determined by melanization; genotyes are experiment *Gyc89Db-GAL4/UAS-Gyc88ERNAi*, n=45 and
619 control *Gyc89Db-GAL4/+*. n=45. Individual value plot with mean and standard deviation, two-way
620 ANOVA.

621 (B) Phagocytosis lineage tracing, effect of *Gyc88E* RNAi in sensory cone neurons on
622 transdifferentiation; genotypes are experiment *21-7-GAL4, UA5-CD8-GFP, Hml*Δ*-DsRed/+; BcF6-*
623 *GFP/ UAS-Gyc88ERNAi*, n=11 and control *21-7-GAL4, UA5-CD8-GFP, Hml*Δ*-DsRed/+; BcF6-*
624 *GFP/+*, n=16. Bar chart with mean and standard deviation, two-way ANOVA.

625 (C) Effect of hypoxia (5% O2) on crystal cell number per larva determined by melanization;
626 genotype is w^{1118}; hypoxia n=46 and normoxia n=48. Individual value plot with mean and standard
627 deviation, two-way ANOVA.

628 (D) Phagocytosis lineage tracing, effect of hypoxia (5% O2) on transdifferentiation; genotype is
629 *Hml*Δ*-GAL4, UAS-GFP; BcF6-mCherry*; hypoxia n=14 and normoxia n=15. Bar chart with mean and
630 standard deviation, two-way ANOVA.

631 (E) Model. Sensory cone neurons detect oxygen by cytoplasmic Gyc heterodimeric oxygen sensors.
632 Gycs convert GTP to cGMP, which activates CNG channels, resulting in influx of calcium (Ca2+)
633 leading to downstream signaling and neuronal activation. Active neurons induce plasmatocyte-to-
634 crystal cell transdifferentiation.

635

636

637

638

639 **Supplemental Materials**

640

641 **Supplemental Figure 1. Methods of crystal cell labeling**

642 (A) Heat induced melanization of crystal cells. Genotype is *lz-GAL4;UAS-GFP*

643 (B) Fluorescent reporter labeling to visualize, and quantify, crystal cells. Genotype is *lz-GAL4;UAS-*
644 *GFP*. Note that the labeled crystal cell pattern by both methods is very similar.

645

646 **Supplemental Figure 2. Limited transient sensory neuron silencing does not affect total**
647 **hemocyte numbers**

648 (A) Transient silencing of sensory neurons, quantification of total hemocytes; genotypes are *21-7-*
649 *GAL4, UAS-CD8-GFP, Hml*Δ*-DsRed/ UAS-Kir2.1; tubGAL80ts/* + , n=12 and control *21-7-GAL4,*
650 *UAS-CD8-GFP, Hml*Δ*-DsRed/ +; tubGAL80ts/* +, n=13. Larvae induced at 29˚C for 22h. Mean and
651 standard deviation, two-way ANOVA

652

653 **Supplemental Figure 3. Hypoxia affects crystal cell counts but not total hemocyte numbers**

654 (A) Effect of 8% hypoxia on crystal cell number determined by melanization; genotype is *w1118*;
655 hypoxia n=19 and normoxia control n=18. Individual value plot with mean and standard deviation,
656 two-way ANOVA.

657 (B) Total hemocyte number under conditions of hypoxia (5% O2) and normoxia; genotype is *Hml*Δ-
658 *GAL4, UAS-GFP; BcF6-mCherry*; hypoxia n=14 and normoxia control n=14. Mean and standard
659 deviation, two-way ANOVA.

660

661 **Supplemental Figure 4. Models**

662 (A) Stimulated by oxygen, activated sensory cone neurons produce signal/s that drive
663 transdifferentiation of a fraction of plasmatocytes to crystal cells. According to this model,
664 transdifferentiation is triggered by contacting the sensory neuron signal, therefore plasmatocytes in
665 anatomical proximity to the sensory cone neurons are most likely to convert into crystal cells.

666 (B) Model illustrating exposure of the caudal end of *Drosophila* larvae including the sensory cones
667 and posterior spiracles to the air, while burying in food. Mature larvae leave the food in preparation
668 of pupariation, now fully exposed to the air.

669

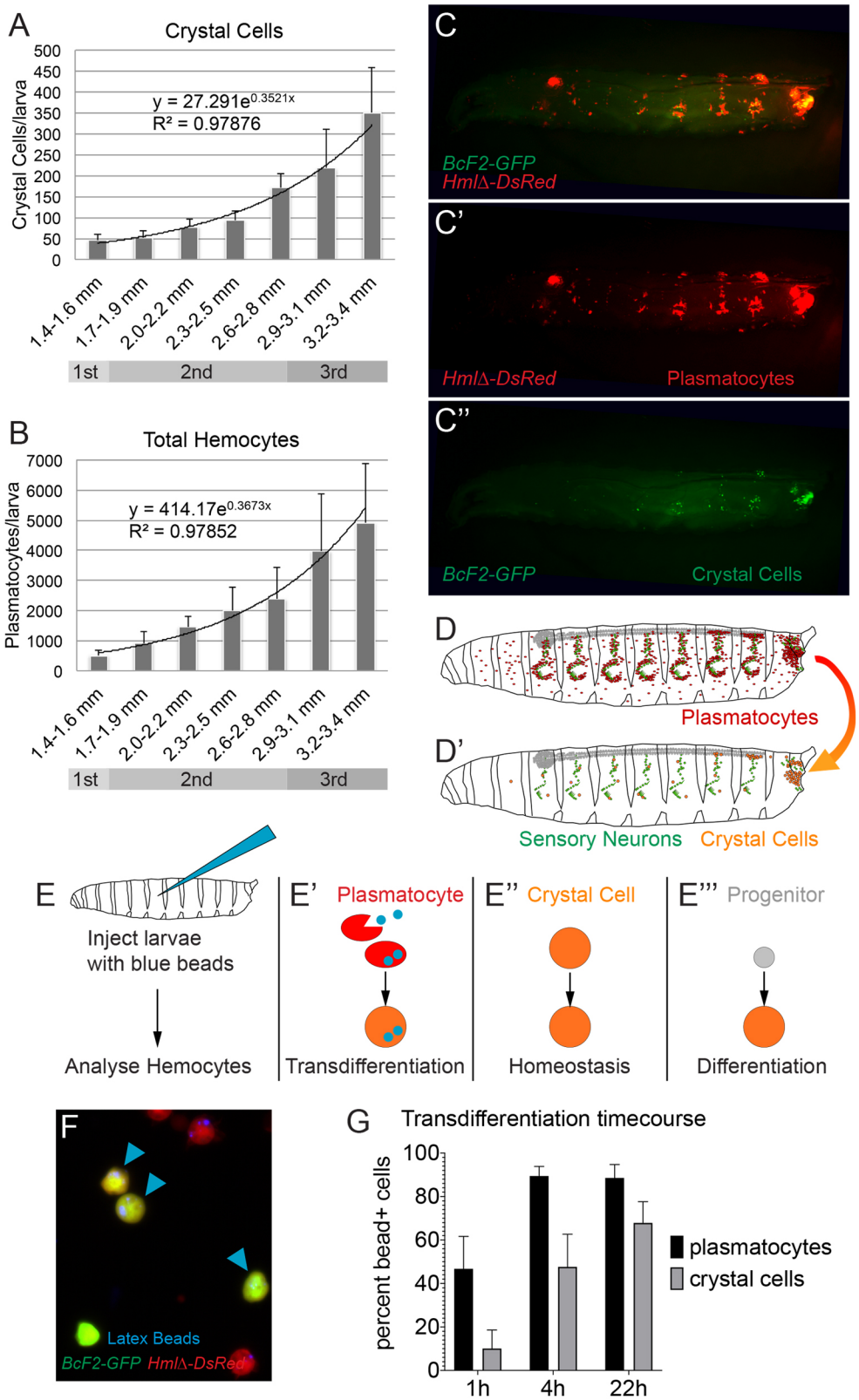

Corcoran et al., Figure 1

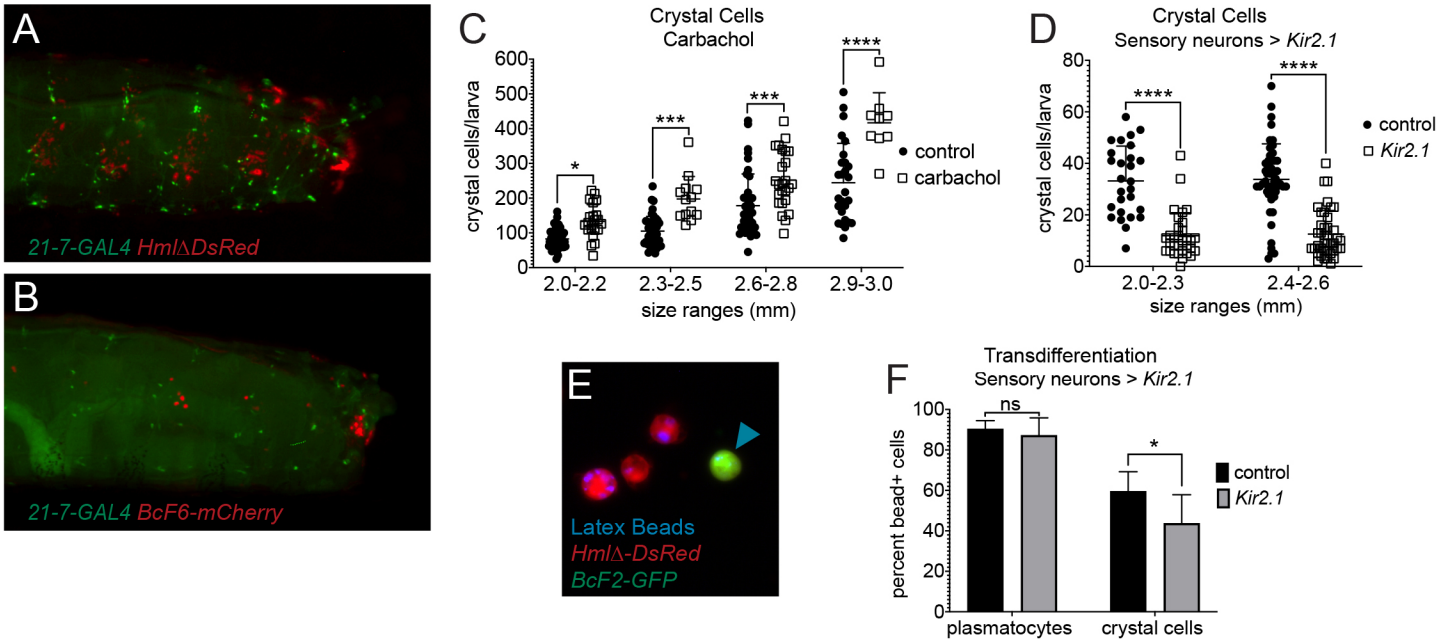

Corcoran et al. Figure 2

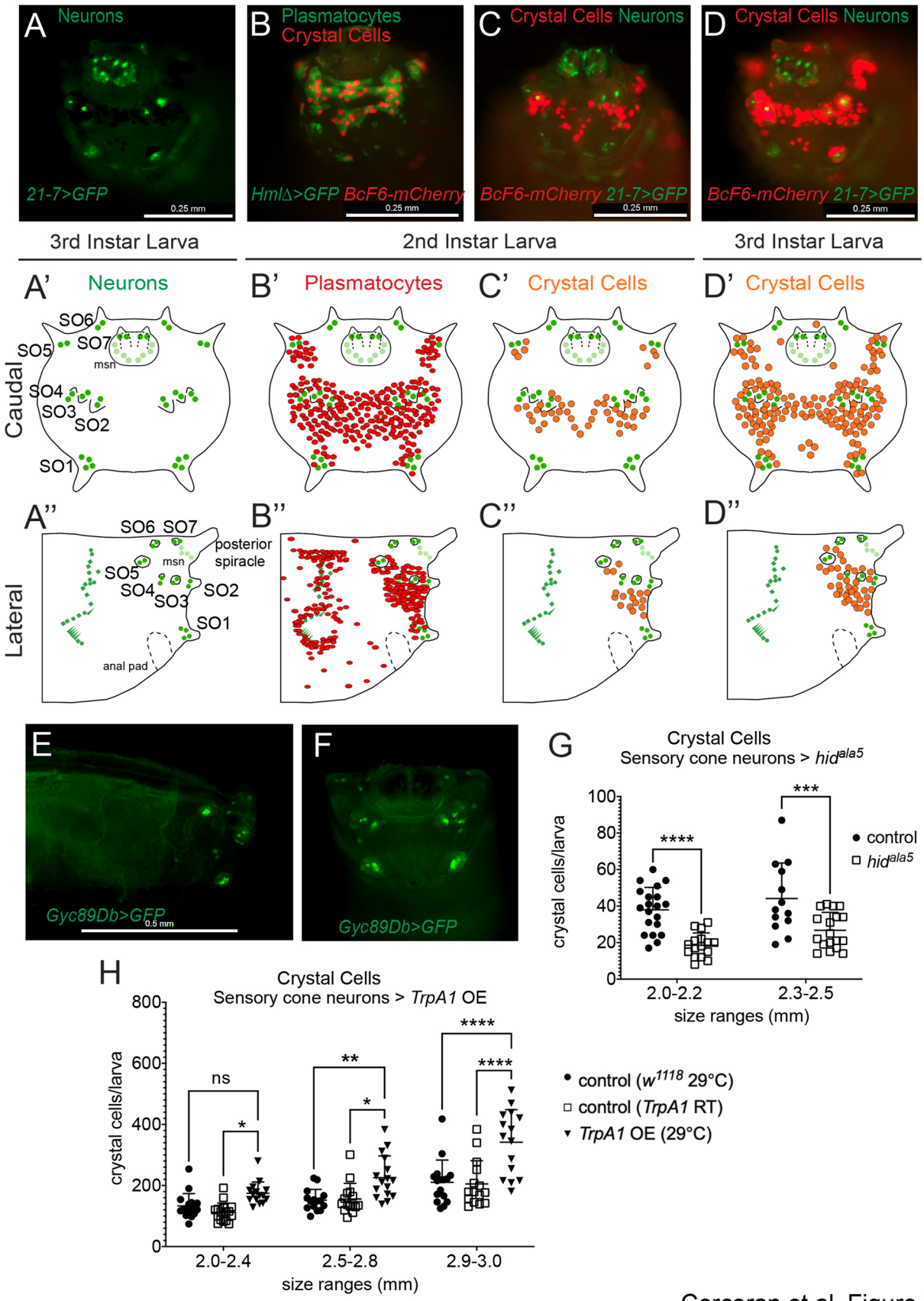

Corcoran et al. Figure 3

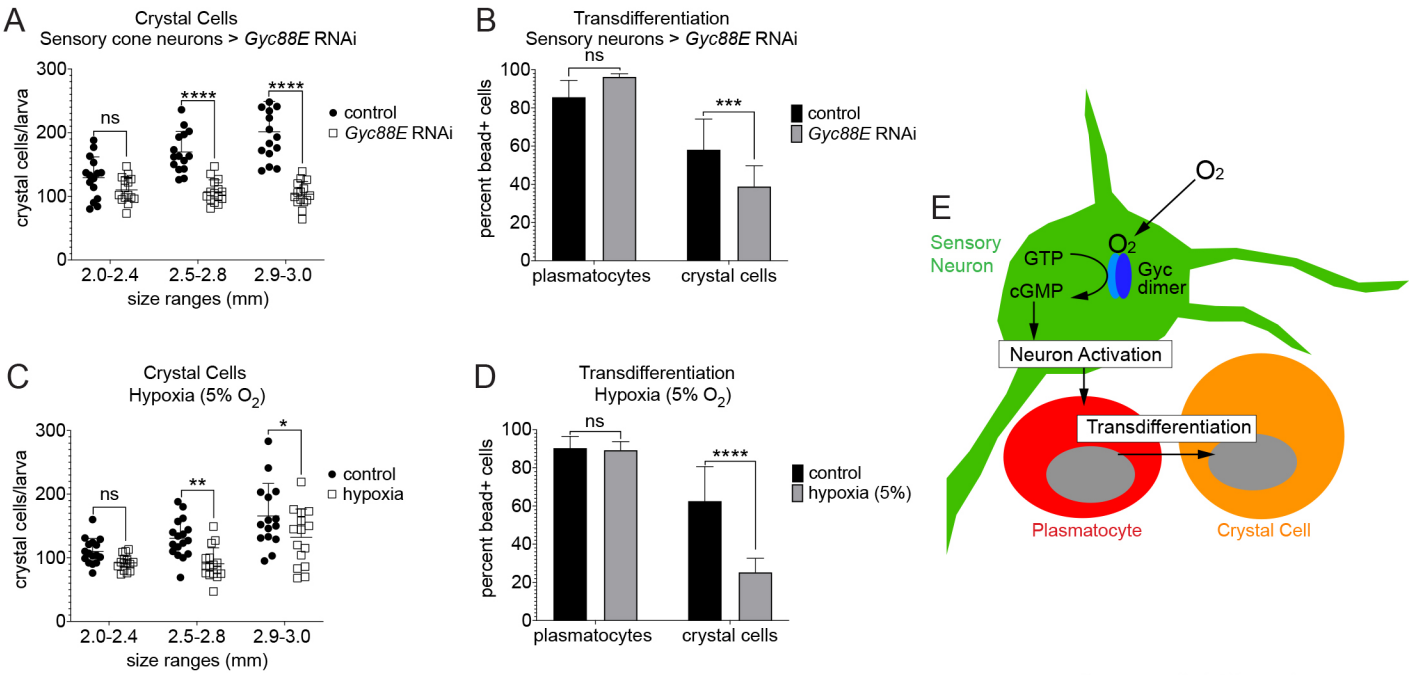

Corcoran et al. Figure 4

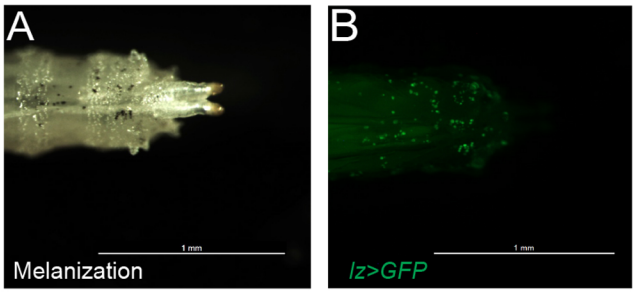

Corcoran et al. Supplemental Figure 1

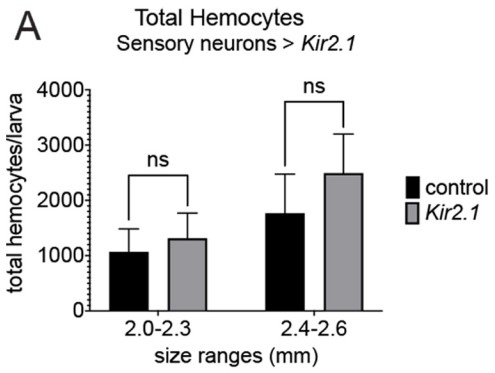

Corcoran et al. Supplemental Figure 2

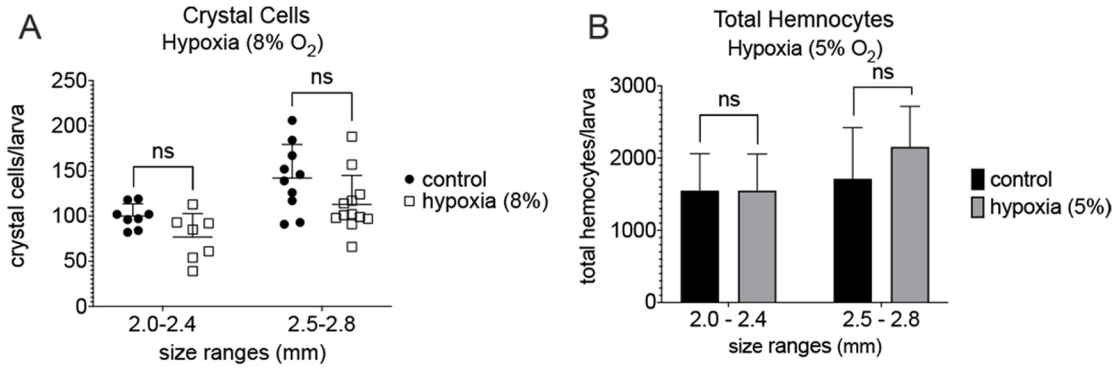

Corcoran et al. Supplemental Figure 3

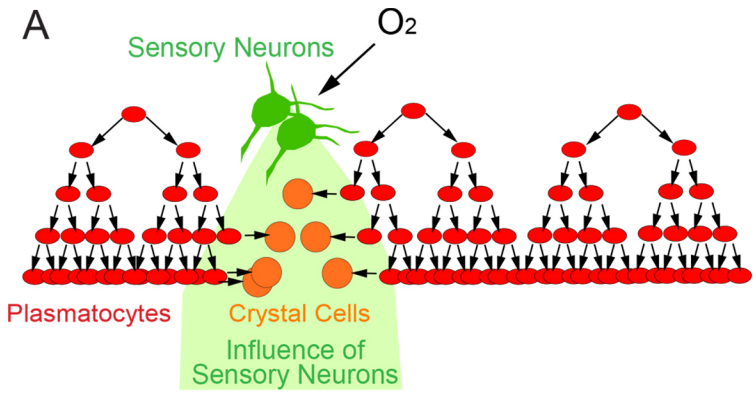

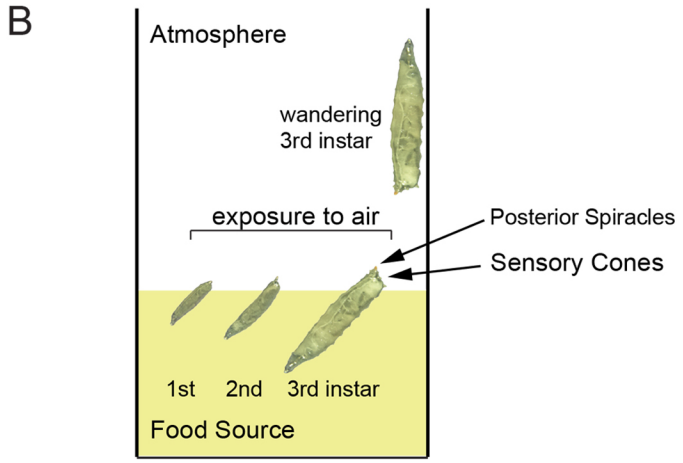

Corcoran et al. Supplemental Figure 4